# An Analysis of the Short-Term Time Stability of the Starlink Ku-Band Downlink Frame Clock

Wenkai Qin*, Zacharias M. Komodromos†, Todd E. Humphreys*
*Department of Aerospace Engineering and Engineering Mechanics, The University of Texas at Austin
†Department of Electrical and Computer Engineering, The University of Texas at Austin

***Abstract*—We develop a signal capture and analysis technique for extracting precise timing information from the Starlink communications megaconstellation's downlink transmissions. Several characterizations of the Starlink frame clock adjustment pattern and stability are presented. The frame clock is adjusted at a regular 1 Hz cadence, and the adjustments are nearly discontinuous in nature. A composite clock Allan deviation analysis indicates that the Starlink frame clock has best-case stability charactersitic of a temperature-controlled crystal oscillator. A further high-frequency clock instability analysis is conducted via polynomial trend removal, and indicates that the Starlink frame clock could hypothetically support a global position, navigiation, and timing (PNT) mission when performing nominally, but manifests episodic oscillatory and excursive behavior that would severely degrade opportunistic positioning and timing based on pseudoranges formed from the frame clock. Examples of such oscillatory and excursive patterns are shown and other aspects of the phenomena are discussed.**

***Index Terms*—Starlink, signal characterization, positioning, time synchronization, low Earth orbit**

## I. Introduction

Global navigation satellite system technology (GNSS) is currently the most prevalent used for positioning, navigation, and timing (PNT). However, traditional GNSS is vulnerable to jamming and spoofing attacks that can leave users without the ability to navigate or synchronize time [1], and threats to traditional GNSS are multiplying dramatically [2]–[4]. According to OPSGROUP, an international association of air transport professionals, GNSS spoofing incidents increased by 500% from 2023 to 2024 [4]. To strengthen radionavigation, researchers have recently focused on augmenting traditional GNSS with large low Earth orbit (LEO) communications constellations [5], with some proposing a combined communications-PNT service for future constellations [6]. Because these constellations offer higher power and wider bandwidth, they are inherently resilient to adversarial interference. Further, the two-way high-rate connectivity afforded by broadband communications constellations enables desirable features such as user authentication and near-zero age of ephemeris and clock models.

Researchers interested in a free-to-use radionavigation receiver have investigated opportunistic approaches to PNT, i.e., PNT extraction with no direct cooperation from the constellation operator and limited *a priori* knowledge regarding satellites' ephemerides and signals. SpaceX's Starlink constellation is of particular interest: it offers the widest signal availability, serving millions of subscribers worldwide with its 7,000+ satellites [7]. Opportunistic approaches using Starlink's Ku-band signals (10.7-12.7 GHz) have already proven fruitful: researchers in several groups have independently demonstrated Doppler-based positioning with accuracy on the order of 10 m [8]–[14]. Unfortunately, Doppler-based techniques cannot approach the exquisite timing precision offered by traditional GNSS: even in the optimistic scenarios posed in [13], [14], timing accuracy is limited to no better than 0.1 ms. By contrast, pseudorange-based PNT from Starlink holds the potential for both meter-accurate positioning and ns-accurate timing [6], [15]. But whether Starlink signals could support precise pseudorange-based PNT remains an open question whose answer depends on the details of the broadcast signals, including modulation, timing, and spectral characteristics.

The authors of [16] uncovered key information regarding the Starlink downlink frame structure, synchronization sequences, and spectral characteristics. Follow-on work in [17] and [18] discovered other predictable elements of each frame, and [19] revealed that Starlink beam switching occurs at 15-s, approximately-GPS-aligned intervals. Other studies have shown simulated impacts of various clock types in LEO [20], or have developed methods for predicting LEO clock corrections, such as those developed for the GRACE mission [21], [22]. Nonetheless, no prior work has characterized the stability of the Starlink frame timing, nor investigated its precise relationship to an absolute time scale such as GPS time (GPST), despite these essential details being prerequisite to development of Starlink-based PNT, whether opportunistic or not.

In this paper, we leverage the insights offered by [16] as well as a dual Starlink and GPS L1 C/A capture system to conduct a detailed study of the Starlink timing properties and makes several contributions elucidating the nature of Starlink's timing characteristics. Note that [16] already details the signal model and capture system used, and thus the related descriptions are forgone. Interested readers are encouraged to refer to [16]. This paper evluates the short-term frame clock stability, defined as the set of clock behaviors that manifest on the order of several seconds or less whose study indicates both the quality of crystal oscillator(s) onboard the Starlink satellite vehicles (SVs) and the predictability of any onboard clock corrections.

## II. System Models and Concepts

This section presents a model for the structure and timing concept framework that will be used to discuss the methods

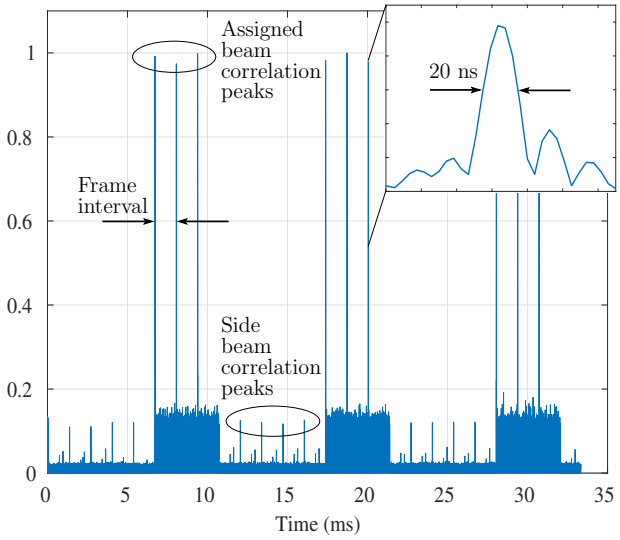


Fig. 1: Normalized cross-correlation of received Starlink data against a local PSS + SSS replica yields sharp peaks at the beginning of each frame whose primary lobe is approximately 20 ns wide for a 55-MHz-bandwidth capture. The nominal interval between frames is $T_\mathrm{f} = 1/750$ s. The strong correlation peaks shown correspond to signals from a beam assigned to the receiver's service cell (assigned beam), whereas the weaker peaks correspond to signals from beams directed toward other service cells (side beams). The assigned beam signal's pre-correlation SNR over this interval is approximately 21 dB. The data shown are for STARLINK-30580, a Block v2.0-Mini SV, from signals captured in February 2024, but the frame correlation pattern is broadly representative of signals captured since 2022 for Blocks v1.0, v1.5, and v2.0-Mini.

and results presented in the following sections. Terminology useful for clear representation of the captured data is first introduced. Then, a theoretical Starlink clock model based on well-established clock models is presented to describe and understand the timing aspects of frame transmission and receipt.

### A. Terminology

To better describe the beams and signals present when opportunistically extracting PNT information from a LEO mega-constellation, we illustrate common data capture complications, reiterate terms presented in previous publications, and introduce several new terms.

We often captured signals that simultaneously included transmissions from both assigned and side beams, as shown in Fig. 1. Such captured signals, referred to as *composite signals* included as many as four coexisting signals and required careful disambiguation. The data presented in this paper all originate from each composite signal's strongest transmission from a single beam, referred to as the *dominant signal*.

### B. Clock Models

As with any analysis of PNT systems based on radio wave propagation, unambiguous and precise models of the various

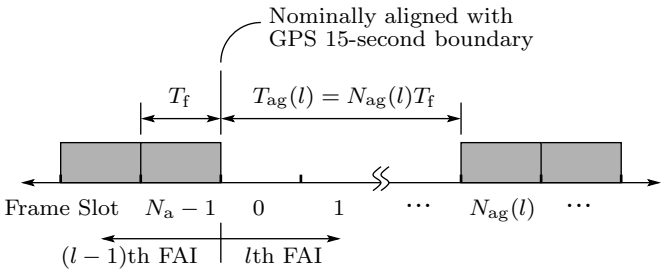


Fig. 2: Frame sequence timing diagram.

clocks involved are key to understanding and characterizing the system. Let $t$ represent true time, or time according to an ideal clock, such as is closely realized by GPS system time [23]. Let $t_\mathrm{f}$ represent time according to a satellite's frame clock, or the clock that governs the timing of frames transmitted by the satellite. Finally, let $t_\mathrm{r}$ represent time according to the receiver clock. These time representations may be related by

$$t = t_\mathrm{f}(t) - \delta t_\mathrm{f}(t) \tag{1}$$

$$t = t_\mathrm{r}(t) - \delta t_\mathrm{r}(t_\mathrm{r}) \tag{2}$$

The frame clock offset $\delta t_\mathrm{f}(t)$ and the receiver clock offset $\delta t_\mathrm{r}(t_\mathrm{r})$ are respectively the amount by which frame time and receiver time lag true time $t$. The receiver clock offset $\delta t_\mathrm{r}(t_\mathrm{r})$ is represented as a function of $t_\mathrm{r}$ because it is natively measured in receiver time in the course of solving for a position and time solution. The frame clock offset $\delta t_\mathrm{f}(t)$ is taken to be function of $t$ because a model for it must be shared among users, which requires a common time base.

The time derivative of $\delta t_\mathrm{f}(t)$ and of $\delta t_\mathrm{r}(t_\mathrm{r})$, both with respect to $t$ and denoted $\dot{\delta t}_\mathrm{f}(t)$ and $\dot{\delta t}_\mathrm{r}(t_\mathrm{r})$, are called the frame and receiver clock drift. They are equivalent to the instantaneous fractional frequency deviation, written generically as $y(t)$, on which clock stability analysis is based [24, Chapter 9].

The time-domain signal $x(t)$ introduced in [16, Section III-A] models the sequence of frames transmitted by a given satellite under the assumption of an ideal clock. With the introduction of $t_\mathrm{f}$, it may be expressed more realistically as $x(t_\mathrm{f})$. Fig. 2 offers further details about the frame clock. Each frame as transmitted has duration $T_\mathrm{f}$ according to the frame clock. Within each FAI, the frame slot index increments from 0 to $N_\mathrm{a} - 1$, with $N_\mathrm{a} = 11250$ being the number of frame slots in a FAI. Each FAI starts at the beginning of frame slot 0 and lasts $N_\mathrm{a}T_\mathrm{f} = 15$ seconds. The interval of unoccupied frame slots at the beginning of each FAI, called the FAI guard interval $T_\mathrm{ag}(l) = N_\mathrm{ag}(l)T_\mathrm{f}$, spans a variable number of frame slots $N_\mathrm{ag}(l) \in [16, 26]$. Note that, for any FAI index $l$, frame slot $N_\mathrm{ag}(l)$ is occupied by definition, but other frame slots may not be occupied.

Let $t_\mathrm{f}(l, m)$ be the frame clock time at the instant when the frame in the $m$th frame slot of the $l$th FAI begins to pass through the phase center of the satellite's downlink antenna, where $l$ and $m$ are zero-based indices. This will be defined as

$$t_\mathrm{f}(l, m) \triangleq 15l + mT_\mathrm{f} \tag{3}$$

The quantity $\delta t_{\mathrm{f}}(l,m)$ is the corresponding clock offset and $t^*(l,m)$ is the corresponding true time, such that $t^*(l,m) = t_{\mathrm{f}}(l,m) - \delta t_{\mathrm{f}}(l,m)$. Another of this paper's key findings is that $\delta t_{\mathrm{f}}(l,0) \approx 0$. Stated differently, a Starlink satellite's frame clock departure from true time at the beginning of each FAI is small—typically less than a few ms.

The quantity $t_{\mathrm{r}}(l,m)$ will be taken to indicate the time of reception, according to the receiver clock, of the frame that was transmitted at true time $t^*(l,m)$, with $\delta t_{\mathrm{r}}(l,m)$ being the corresponding receiver clock offset and $t_*(l,m)$ being the corresponding true time. More precisely, $t_{\mathrm{r}}(l,m)$ is the receiver clock time at which the frame transmitted at $t^*(l,m)$ from the satellite's downlink antenna's phase center first reached the receiver antenna's phase center. The receipt time $t_{\mathrm{r}}(l,m)$ can be related to $t_*(l,m), t^*(l,m)$, and $t_{\mathrm{f}}(l,m)$ by

$$t_*(l,m) = t_{\mathrm{r}}(l,m) - \delta t_{\mathrm{r}}(l,m) \tag{4}$$

$$t^*(l,m) = t_{\mathrm{r}}(l,m) - \delta t_{\mathrm{r}}(l,m) - \delta t_{\mathrm{tof}} \tag{5}$$

$$t_{\mathrm{f}}(l,m) = t_{\mathrm{r}}(l,m) - \delta t_{\mathrm{r}}(l,m) - \delta t_{\mathrm{tof}} + \delta t_{\mathrm{f}}(l,m) \tag{6}$$

where $\delta t_{\mathrm{tof}}$ is the frame's true time of flight from transmission to reception.

## III. Data Preprocessing

We capture Starlink signals at a complex sampling rate ranging from 50.0 to 62.5 MHz. Captured signals are then upsampled to the Starlink information symbol rate $F_{\mathrm{s}} = 240$ MHz so that all subsequent operations may proceed as if the full 240-MHz Starlink channel bandwidth had been captured. The upsampled signal is cross-correlated against a local signal replica consisting of the coherent PSS + SSS combination to produce correlation peaks like those shown in Fig. 1. For the $m$th frame, let

$$x_{m01}(t) \triangleq \begin{cases} x_{m0}(t), & 0 \le t < T_{\mathrm{sym}} \\ x_{m1}(t - T_{\mathrm{sym}}), & T_{\mathrm{sym}} \le t < 2T_{\mathrm{sym}} \\ 0, & \text{otherwise} \end{cases} \tag{7}$$

be the coherent concatenation of the time-domain PSS and SSS functions from [16]. Because the PSS and SSS are present in all Starlink downlink frames and are identical for all frames $m \in \mathbb{Z}$ and all SVs, $x_{m01}(t)$ can be used for correlation against all captured data.

The full discrete-time local signal replica used for correlation is the product of $x_{m01}(t)$ and a complex exponential:

$$y_{m01}[k] \triangleq x_{m01}(kT_{\mathrm{s}}(1-\beta)) \exp\left(j2\pi \left[F_{\mathrm{c}}(1-\beta) - \bar{F}_{\mathrm{c}}\right] kT_{\mathrm{s}}\right) \tag{8}$$

Here, $T_{\mathrm{s}} = 1/F_{\mathrm{s}}$ is the sampling interval, $F_{\mathrm{c}}$ is the center frequency of the OFDM channel, $\beta$ is the CFO parameter, and $\bar{F}_{\mathrm{c}} \approx F_{\mathrm{c}}$ is the center frequency to which the receiver is tuned. Correlation proceeds in blocks of between 30 and 60 frame intervals $T_{\mathrm{f}}$. Over each block, a constant $\beta$ is applied that maximizes correlation peak magnitudes within the block. This process amounts to batch sequential frequency tracking.

A high-precision TOA measurement is extracted from the correlation peak for each frame received. Unless otherwise noted, all frame timing measurements were extracted from dominant signals with pre-correlation SNR exceeding -1 dB, which, upon correlation against the replica signal in (8), yields a post-correlation SNR of at least 25 dB for a $\ge$ 50-MHz captured bandwidth [25]. Let $\mathcal{M}_l$ be the set of occupied-frame indices for the $l$th FAI. A sequence of frame TOA measurements corresponding to $\mathcal{M}_l$ is extracted from the cross-correlation function. These are modeled as

$$\tilde{t}_{\mathrm{r}}(l,m) = t_{\mathrm{r}}(l,m) + w_{\mathrm{r}}(l,m), \quad m \in \mathcal{M}_l \tag{9}$$

where $w_{\mathrm{r}}(l,m)$ is zero-mean Gaussian measurement error with variance $\sigma_w^2(l,m)$. The $m$th measurement $\tilde{t}_{\mathrm{r}}(l,m)$ is the receiver time of the discrete sample instant at which the correlation peak for the $m$th frame is maximized. As can be appreciated by examining the zoomed inset in Fig. 3, the measurement errors $\{w_{\mathrm{r}}(l,m) \mid m \in \mathcal{M}_l\}$ contain errors due to (1) nearest-sample quantization of the maximizing location, (2) thermal noise, and (3) peak rounding caused by filtering in the RFSA for the relatively narrow bandwidth captured (e.g., 55 MHz for Fig. 1 as compared to the full $F_{\mathrm{s}} = 240$-MHz bandwidth).

## IV. Short-Term Frame Clock Stability

This section presents findings regarding short term (within a single FAI) Starlink frame clock behavior. Rearranging (6) to isolate $\delta t_{\mathrm{f}}(l,m)$ yields

$$\delta t_{\mathrm{f}}(l,m) = t_{\mathrm{f}}(l,m) - t_{\mathrm{r}}(l,m) + \delta t_{\mathrm{r}}(l,m) + \delta t_{\mathrm{tof}}(l,m) \tag{10}$$

Let $\delta t'_{\mathrm{f}}(l,m)$ be equivalent to $\delta t_{\mathrm{f}}(l,m)$ but with a 3rd-order polynomial fit across all $m \in \mathcal{M}_l$ removed. Assume like notation for the other terms in (10). Analysis of $\delta t'_{\mathrm{f}}(l,m)$ is sufficient to characterize the short-term properties of the frame clock because $\delta t'_{\mathrm{f}}(l,m)$ retains the high-frequency variations present in $\delta t_{\mathrm{f}}(l,m)$. The detrended $\delta t_{\mathrm{f}}(l,m)$ can be modeled as

$$\begin{aligned} \delta t'_{\mathrm{f}}(l,m) &= t'_{\mathrm{f}}(l,m) - t'_{\mathrm{r}}(l,m) + \delta t'_{\mathrm{r}}(l,m) + \delta t'_{\mathrm{tof}}(l,m) \\ &\approx -t'_{\mathrm{r}}(l,m) \\ &\approx -\tilde{t}'_{\mathrm{r}}(l,m) \end{aligned} \tag{11}$$

This approximation is explained as follows: For $m \in \mathcal{M}_l$, $t_{\mathrm{f}}(l,m)$ is an affine function of $m$, which implies $t'_{\mathrm{f}}(l,m) = 0$. Likewise, $\delta t'_{\mathrm{r}}(l,m) \approx 0$ because the receiver clock is a GPS-disciplined OCXO with negligible frequency error. Finally, $\delta t'_{\mathrm{tof}}(l,m) \approx 0$ because the time of flight to an SV in LEO can be modeled to better than 1 ns over a 15-s FAI as a 3rd-order function.

In summary, for purposes of a short-term frame clock stability analysis, $\delta t'_{\mathrm{f}}(l,m)$ is a valid proxy for $\delta t_{\mathrm{f}}(l,m)$, and $\tilde{t}'_{\mathrm{r}}(l,m)$, the 3rd-order-polynomial-detrended version of the frame TOA measurement $\tilde{t}_{\mathrm{r}}(l,m)$, is equivalent to $\delta t'_{\mathrm{f}}(l,m)$ to within a sign reversal and the ns-level measurement error $w_{\mathrm{r}}(l,m)$.

Note that until near the end of this section, we limit our analysis to v1.0 and v1.5 SVs, as their frame clocks behave differently from those of v2.0-Mini SVs.

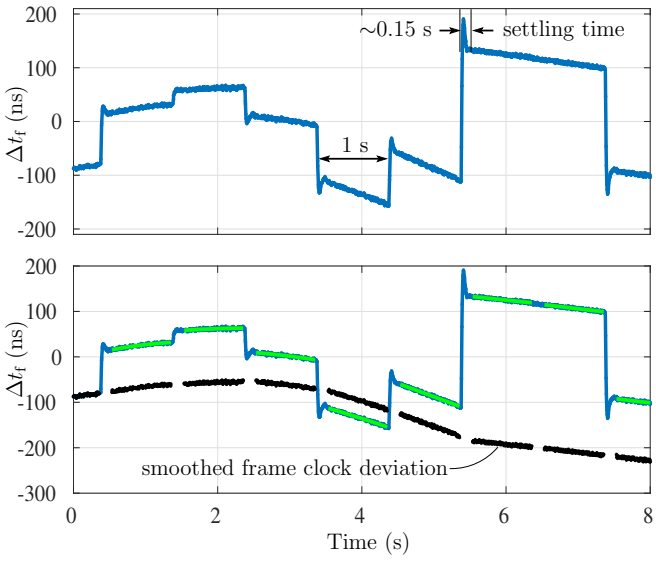


Fig. 3: Top: $\tilde{t}'_r$ vs. $t_f$ for an example capture occurring within a single FAI. Bottom: $\tilde{t}'_r$ (blue), piecewise 2nd-order polynomial fits to the truncated inter-adjustment segments (green), and $\tilde{t}''_r$, truncated inter-adjustment segments with first-order discontinuity eliminated (black). The data shown are for STARLINK-5141, a v1.5 SV, from signals captured in November 2023.

### A. Periodic Frame Clock Adjustments

The top panel of Fig. 3 shows an example $\tilde{t}'_r$ trace for an 8-s interval within a single FAI. Interpreting $\tilde{t}'_r$ as a proxy for the detrended frame clock deviation $\delta t'_f$, it is clear that the Starlink frame clock exhibits abrupt adjustments at a regular 1-Hz cadence. We believe these are the result of coarse GNSS disciplining of the base oscillator. Similar adjustments at the same 1-Hz cadence were evident in every capture of signals from Starlink v1.0 and v1.5 SVs. If due to GNSS disciplining, such large and frequent adjustments—up to several hundred ns at 1 Hz—reflect a base oscillator with poor stability.

Abrupt and coarse adjustments to the frame clock are obviously undesirable for pseudorange-based PNT. Unless they can be modeled or eliminated by some differential scheme, such adjustments would cause large errors in pseudorange modeling, and thus in position and timing estimation. They act, in effect, like the clock dithering implemented to intentionally degrade GPS accuracy under the Selective Availability program discontinued in May 2000 [26].

To assess their predictability and other characteristics, we analyzed 281 adjustments associated with 12 unique Starlink v1.0 and v1.5 SVs and made the following observations.

*1) Cadence:* Frame clock adjustment opportunities occur at an almost perfectly regular 1-Hz cadence. Of the 281 adjustments studied, all but one arrived within a few ms of an integer second from the previous one, according to the frame clock $t_f$. The single outlier, from a STARLINK-5666 (v1.5) capture, arrived 100 ms earlier than expected. At each opportunity, an adjustment may occur or not—note the lack of adjustment at 6.5 s in Fig. 3.

*2) Probability Distribution of Adjustment Amplitudes:* If the 1-Hz frame clock adjustments were quantized (say, occurring only in 20-ns steps), this would offer hope of developing an adjustment compensation mechanism within a pseudorange-based position and time estimator. Alas, this is not the case. Instead, the adjustment amplitudes appear to be smoothly distributed with mean $\mu_a = 20$ ns and standard deviation $\sigma_a = 117$ ns. A Shapiro-Wilk goodness-of-fit test for normality yielded $p = 0.3$, suggesting a reasonably close alignment with the Gaussian distribution [27].

### B. Nominal Jitter

A further processing step allows us to assess the high frequency variations (jitter) in $\tilde{t}_r$. We subtract from $\tilde{t}'_r$ the 2nd-order polynomial fits (the green segments in Fig. 3) of each truncated inter-adjustment segment to flatten the time series. We denote this flattened time series as $\tilde{t}'''_r$, an example of which is shown in the top plot of Fig. 4. Under nominal conditions for v1.0 and v1.5 SVs, the RMS value of $\tilde{t}'''_r$ ranges between 1.7 and 2.5 ns. A large contributor to this jitter is nearest-sample quantization noise, which, for $y_{m01}[k]$ from (8) sampled at $F_s = 240$ MHz, has an RMS value of $1/\sqrt{12}F_s = 1.2$ ns [28]. Assuming this noise is independent of other sources of jitter, the RMS contribution of the other sources ranges from 1.5 to 2.2 ns. Some of this is due to thermal noise in the receiver, so 2.2 ns serves an an upper bound on the jitter in the SVs' frame clock deviation $\delta t_f$ under nominal behavior. This implies that the frame clock of Starlink v1.0 and v1.5 SVs is capable of maintaining jitter at the ns level, which, setting aside the 1-Hz time and frequency adjustments and the lower-frequency variations in $\delta t_f$, is adequately low to support accurate pseudorange-based PNT.

### C. Short-Term Frame Clock Stability Bound

To probe the stability limits of the v1.0 and v1.5 Starlink SV frame clocks, we performed an Allan deviation analysis of 18 smoothed frame time histories similar to the black trace in Fig. 3. The duration of these time histories ranged from 10 to 15 seconds. The data originate from 9 unique Block v1.0 and v1.5 Starlink SVs whose signals were captured during 2022 and 2023 and whose frame timing was derived from assigned beams, insofar as could be ensured, and manifested no anomalous excursions besides the 1-Hz clock correction discontinuities. Given the processing and data selection involved in creating the smoothed frame time histories on which the composite Allan deviation was based, which includes not only removal of orbital effects but also some low-frequency clock deviations, the Allan deviation analysis should be taken as a lower bound on the frame clock stability of Block v1.0 and v1.5 Starlink SVs. This Allan deviation analysis shows that the Starlink frame clock possesses best-case behavior broadly consistent with a temperature-compensated crystal oscillator (TCXO). For example, at an averaging time of 1 second, the fractional frequency stability $\sigma_y(\tau) = 2.5 \times 10^{-9}$, which is what one would expect from an average-quality TCXO at $\tau = 1$ second. Thus, we may conclude that the frame clock stability of the Starlink v1.0 and v1.5 frame clocks is no better than a TXCO, though, as will be discussed below, it can episodically be much worse.

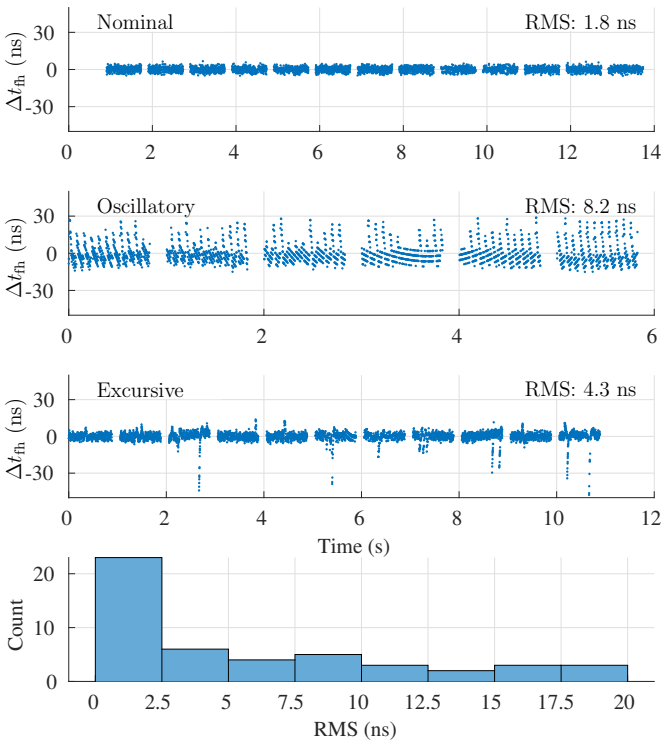


Fig. 4: Top three panels: The flattened time series $\tilde{t}_{\mathrm{r}}'''$ for the same Starlink SV during three contiguous FAIs, showing nominal, oscillatory, and excursive high-frequency frame clock behavior. The data shown are for STARLINK-2119, a v1.0 SV, from signals captured in November 2023. Bottom panel: Histogram of per-FAI $\tilde{t}_{\mathrm{r}}'''$ RMS values for all v1.0 and v1.5 SVs studied. A single RMS measurement was extracted from the $\tilde{t}_{\mathrm{r}}'''$ time history corresponding to the dominant signal of each FAI.

### D. Anomalous Frame Clock Behavior

The foregoing jitter and stability results apply only for nominal behavior of the Starlink frame clock, which holds for approximately half of the FAIs studied. The other half manifest various modes of high-frequency frame clock instability. We do not know the underlying cause of these anomalous frame clock behavior modes, but we note here certain patterns of behavior and offer conjectures about their meaning.

Consider the top three panels of Fig. 4, which show the flattened time series $\tilde{t}_{\mathrm{r}}'''$ for 10-s intervals within three separate FAIs. The top panel shows nominal behavior, with 1.8 ns RMS, and acts as a baseline for comparison. The second panel shows much higher-RMS variations with significant time correlation. In this example trace, the deviations are bounded between $-13$ ns and 28 ns and include strong frequency components at 7.2 and 13.7 Hz. We classify anomalous frame clock behavior as oscillatory, as in this example, when one or two spectral components dominate. The third panel shows a $\tilde{t}_{\mathrm{r}}'''$ time history with sudden and irregularly spaced deviations, e.g., at the 2.6 s and 5.4 s marks. We classify such behavior as excursive.

The bottom panel of Fig. 4 shows a histogram of $\tilde{t}_{\mathrm{r}}'''$ RMS values for all v1.0 and v1.5 SVs studied. Each sample contributing to the histogram is a scalar RMS measurement extracted from the $\tilde{t}_{\mathrm{r}}'''$ time history corresponding to the dominant signal of a single FAI. Of the 48 FAIs studied,

- 22 exhibited nominal frame clock behavior, with RMS values below 2.5 ns;
- 19 exhibited oscillatory behavior, with RMS values above 2.5 ns and having a principal frequency component typically residing between 12 and 14 Hz;
- 3 exhibited excursive behavior;
- and 4 exhibited other behaviors, such as a mix of oscillatory and excursive modes, or elevated RMS values but without sudden excursions or dominant frequency components.

A clue to the origin of anomalous frame clock behavior may be found in the following remarkable observation: Whatever mode the frame clock manifests—whether nominal, oscillatory, excursive, or otherwise—invariably persists during a full FAI, but can switch to a different mode in the next FAI, even for the same SV. In fact, the traces in the top three panels of Fig. 4 are for the same Starlink SV during three contiguous FAIs. From this clue we conclude that anomalous behavior is connected to satellite hardware or software configuration changes that occur at FAI boundaries. For example, it may be that each of the three traces in Fig. 4 comes from an assigned beam cast by a different one of the serving Starlink SV's downlink phase arrays, of which each SV has three. If the three phased arrays are driven by separate clocks, each with its own characteristic high-frequency behavior, this would explain the FAI-aligned frame clock mode switching. Alternatively, it may be that the baseband frame assembly process is governed by parameters set in software that remain fixed over each FAI, and that some parameter combinations lead to nominal frame clock behavior whereas others lead to anomalous modes.

As with the 1-Hz clock adjustments, the anomalous frame clock variations discussed here would tend to degrade pseudorange-based PNT solutions formed from frame TOA measurements. While the root cause of anomalous frame clock behavior remains a mystery, we emphasize that nearly half of the FAIs studied showed nominal frame clock jitter, with RMS values below 2.5 ns. Clearly, the Starlink v1.0 and v1.5 baseband frame assembly process, and at least a large fraction of its base oscillators, have sufficient stability to support high-accuracy pseudorange-based PNT, provided the 1-Hz frame clock adjustments could somehow be modeled or eliminated.

### E. Starlink v2.0 Frame Clock

We also generated $\tilde{t}_{\mathrm{r}}'$ time histories for v2.0-Mini SVs. These revealed frame clock adjustment behavior differing from that of v1.0 and v1.5 SVs in two ways: (1) the adjustments' magnitudes were generally much smaller, and (2) the adjustments occurred at irregular intervals, as opposed to the regular 1-Hz intervals for v1.0 and v1.5 SVs. Apparently, the Starlink v2.0-Mini SVs employ a different mechanism for base oscillator GNSS disciplining.

## V. Conclusions

We have developed and used a dual-capture system and accompanying processing technique that simultaneously cap-

tures both Starlink and GPS L1 C/A signals, providing high-precision estimation of the signal time of receipt. With the data provided, we conduct a relative frame timing analysis of the Starlink frame clock and provide characterizations of its clock adjustment and short-term stability. Further, we identify two patterns of clock instability of concern for developers of a Starlink-based PNT receiver.

## Acknowledgments

Research was supported in part by the by the U.S. Department of Transportation under Grant 69A3552348327 for the CARMEN+ University Transportation Center, by Sandia National Laboratories, and by affiliates of the 6G@UT center within the Wireless Networking and Communications Group at The University of Texas at Austin. Sandia National Laboratories is a multimission laboratory managed and operated by National Technology & Engineering Solutions of Sandia, LLC, a wholly owned subsidiary of Honeywell International Inc., for the U.S. Department of Energy's National Nuclear Security Administration under contract DE-NA0003525. This paper describes objective technical results and analysis. Any subjective views or opinions that might be expressed in the paper do not necessarily represent the views of the U.S. Department of Energy or the United States Government.

## References

[1] T. E. Humphreys, "Interference," in *Springer Handbook of Global Navigation Satellite Systems*. Springer International Publishing, 2017, pp. 469–503.

[2] M. J. Murrian, L. Narula, P. A. Iannucci, S. Budzien, B. W. O'Hanlon, S. P. Powell, and T. E. Humphreys, "First results from three years of GNSS interference monitoring from low Earth orbit," *NAVIGATION*, vol. 68, no. 4, pp. 673–685, 2021.

[3] Z. Clements, P. Ellis, and T. E. Humphreys, "Dual-satellite geolocation of terrestrial GNSS jammers from low Earth orbit," in *Proceedings of the IEEE/ION PLANS Meeting*, Monterey, CA, 2023, pp. 458–469.

[4] G. S. Workgroup, "GPS spoofing: Final report of the GPS spoofing workgroup," OPSGROUP, Tech. Rep., 2024. [Online]. Available: https://ops.group/blog/gps-spoofing-final-report

[5] W. Stock, R. T. Schwarz, C. A. Hofmann, and A. Knopp, "Survey on opportunistic PNT with signals from LEO communication satellites," *IEEE Communications Surveys & Tutorials*, 2024.

[6] P. A. Iannucci and T. E. Humphreys, "Fused low-Earth-orbit GNSS," *IEEE Transactions on Aerospace and Electronic Systems*, pp. 1–1, 2022.

[7] P. Gomez-del Hoyo and P. Samczynski, "Starlink-based passive radar for Earth's surface imaging: first experimental results," *IEEE Journal of Selected Topics in Applied Earth Observations and Remote Sensing*, 2024.

[8] Z. M. Kassas, N. Khairallah, and S. Kozhaya, "Ad astra: Simultaneous tracking and navigation with megaconstellation LEO satellites," *IEEE Aerospace and Electronic Systems Magazine*, 2024.

[9] M. Neinavaie and Z. M. Kassas, "Cognitive sensing and navigation with unknown OFDM signals with application to terrestrial 5G and Starlink LEO satellites," *IEEE Journal on Selected Areas in Communications*, 2023.

[10] N. Jardak and R. Adam, "Practical use of Starlink downlink tones for positioning," *Sensors*, vol. 23, no. 6, p. 3234, 2023.

[11] C. Yang and A. Soloviev, "Starlink Doppler and Doppler rate estimation via coherent combining of multiple tones for opportunistic positioning," in *2023 IEEE/ION Position, Location and Navigation Symposium (PLANS)*. IEEE, 2023, pp. 1143–1153.

[12] S. Kozhaya and Z. M. Kassas, "On the fundamental tracking performance and design considerations of radio navigation," *IEEE Journal on Selected Areas in Communications*, 2024.

[13] M. L. Psiaki, "Navigation using carrier Doppler shift from a LEO constellation: TRANSIT on steroids," *NAVIGATION*, vol. 68, no. 3, pp. 621–641, 2021.

[14] M. O. Moore, M. L. Psiaki, and R. M. Buehrer, "Time-diverse Doppler-only LEO PNT: Initial solution," in *Proceedings of the ION GNSS+ Meeting*, 2024, pp. 3532–3541.

[15] P. A. Iannucci and T. E. Humphreys, "Economical fused LEO GNSS," in *Proceedings of the IEEE/ION PLANS Meeting*, 2020.

[16] T. E. Humphreys, P. A. Iannucci, Z. M. Komodromos, and A. M. Graff, "Signal structure of the Starlink Ku-band downlink," *IEEE Transactions on Aerospace and Electronic Systems*, pp. 1–16, 2023.

[17] Z. M. Komodromos, W. Qin, and T. E. Humphreys, "Weak signal acquisition and tracking of the Starlink Ku-Band downlink to enable global PNT," in *Proceedings of the ION Joint Navigation Conference (JNC)*, 2024.

[18] S. Kozhaya, J. Saroufim, and Z. M. Kassas, "Starlink for PNT: A trick or a treat?" in *Proceedings of the 36th International Technical Meeting of the Satellite Division of The Institute of Navigation (ION GNSS+ 2023)*, 2024.

[19] W. Qin, Z. M. Komodromos, and T. E. Humphreys, "An agile, portable antenna system for LEO megaconstellation-based PNT," in *Proceedings of the ION GNSS+ Meeting*, 2023.

[20] K. Wang and A. El-Mowafy, "LEO satellite clock analysis and prediction for positioning applications," *Geo-spatial Information Science*, vol. 25, no. 1, pp. 14–33, 2022. [Online]. Available: https://doi.org/10.1080/10095020.2021.1917310

[21] H. Ge, T. Wu, and B. Li, "Characteristics analysis and prediction of low earth orbit (LEO) satellite clock corrections by using least-squares harmonic estimation," *GPS Solutions*, vol. 27, no. 1, p. 38, 2023.

[22] C. Jiang, Z. Luo, M. Zhu, M. Guan, H. Zhu, and M. Gao, "Characteristics analysis of LEO satellite clock corrections and prediction by sliding estimation," *Available at SSRN 4818891*, 2024.

[23] C. Jekeli and O. Montenbruck, "Time and reference systems," in *Springer Handbook of Global Navigation Satellite Systems*. Springer International Publishing, 2017, pp. 25–58.

[24] A. Thompson, J. Moran, and G. Swenson, *Interferometry and Synthesis in Radio Astronomy*. Wiley, 2001.

[25] Z. M. Komodromos, W. Qin, and T. E. Humphreys, "Signal simulator for Starlink Ku-Band downlink," in *Proceedings of the ION GNSS+ Meeting*, 2023, pp. 2798–2812.

[26] D. Odijk and L. Wanninger, "Differential positioning," in *Springer Handbook of Global Navigation Satellite Systems*. Springer International Publishing, 2017, pp. 753–780.

[27] P. Royston, "Approximating the Shapiro-Wilk W-test for non-normality," *Statistics and computing*, vol. 2, pp. 117–119, 1992.

[28] R. M. Gray and D. L. Neuhoff, "Quantization," *IEEE Transactions on Information Theory*, vol. 44, no. 6, pp. 2325–2383, 1998.